Scientific Research Publishing

Open Journal of Fluid Dynamics, 2022, 12, 263-276
https://www.scirp.org/journal/ojfd
ISSN Online: 2165-3860
ISSN Print: 2165-3852

Analytical Study of the Electroosmotic Flow of Two Immiscible Power-Law Fluids in a Microchannel

Shuyan Deng

Institute of Architecture and Civil Engineering, Guangdong University of Petrochemical Technology, Maoming, China
Email: sydeng4-c@my.cityu.edu.hk

How to cite this paper: Deng, S.Y. (2022) Analytical Study of the Electroosmotic Flow of Two Immiscible Power-Law Fluids in a Microchannel. *Open Journal of Fluid Dynamics*, **12**, 263-276.
https://doi.org/10.4236/ojfd.2022.123013

Received: July 18, 2022
Accepted: September 3, 2022
Published: September 6, 2022

Abstract

The multilayer microchannel flow is a promising tool in microchannel-based systems such as hybrid microfluidics. To assist in the efficient design of two-liquid pumping system, a two-fluid electroosmotic flow of immiscible power-law fluids through a microtube is studied with consideration of zeta potential difference near the two-liquid interface. The modified Cauchy momentum equation in cylindrical coordinate governing the two-liquid velocity distributions is solved where both peripheral and inner liquids are represented by power-law model. The two-fluid velocity distribution under the combined interaction of power-law rheological effect and circular wall effect is evaluated at different viscosities and different electroosmotic characters of inner and peripheral power-law fluids. The velocity of inner flow is a function of the viscosities, electric properties and electroosmotic characters of two power-law fluids, while the peripheral flow is majorly influenced by the viscosity, electric property and electroosmotic characters of peripheral fluid. Irrespective of the configuration manner of power-law fluids, the shear thinning fluid is more sensitive to the change of other parameters.

Keywords

Two-Liquid Electroosmotic Flow, Non-Newtonian Fluids, Circular Wall Effect, Electrokinetic Width, Flow Behavior Index

1. Introduction

With the applications of microfluidic technologies, the microchannel flows have been frequently encountered when manipulating working liquids in the driving devices such as micropumps and micromixers [1] [2]. The remarkable rise of the

surface to volume ratio in microchannels and the immediate contact between the liquid and channel wall induce the formation of electric double layer (EDL) with free charged ions in the vicinity of channel wall. Under the interaction of the EDL and the applied electric field, the liquid molecules near the channel wall will migrate which render the bulk liquid moves forward by viscous shear stress, resulting in the electroosmotic flow (EOF) [3]. On one hand, the EOF was studied in terms of the transport processing in different microchannels [4] [5] [6] [7]. Owing to the advantage of microcapillary geometry in microfluidics, both hydrodynamic and thermal behaviors of EOF in cylindrical microcapillary have been analytically or numerically studied [8] [9]. On the other hand, in biomedical and chemical applications, the liquids with nonlinear constitutive relation have been commonly operated. As compared to Newtonian fluid, the non-Newtonian fluid possesses nonlinear rheological relation between shear stress and shear rate. The fluid viscosity is an inherent characteristic of fluids, which is a function of shear rate for non-Newtonian fluid. Accordingly, the equations proposed for non-Newtonian models are highly nonlinear and complicated. A number of researchers focused on the investigation concerning hydrodynamic behaviors in EOF for both Newtonian and non-Newtonian fluids. More specifically, the EOF considering different nonlinear rheological relations such as the power-law model [10] [11] [12], viscoelastic model [13], Maxwell model [14] and Casson model [15] has been studied. Recently, the studies on EOF were developed to that under various imposed conditions such as an external magnetic field or rotating environment [16] [17] [18]. In further, the advantages of EOF such as the plug-like pattern and convenience of being controlled and integrated in microdevices, were leveraged to develop electroosmotic pumping system (EOP). Using the porous polymer membrane, Gao *et al.* developed a miniature 2 cm^3 EOP [19] and established an analytical prediction method for porous glass EOP [20].

The previous literature focused on the single-fluid EOF of fluids. However, in microfluidic devices, the biofluids and chemical solutions with low electroosmotic (EO) mobility like oil and organic solvents need to be manipulated. Brask *et al.* [21] developed a two-liquid pumping system where the low EO mobility fluid flow was assisted by high EO mobility fluid flow. To efficiently develop two-liquid pumping system, it is fundamentally important to provide an in-depth insight to the immiscible two-fluid flow in microchannel. In addition, the two-Newtonian fluid model was extended to that under varying wall shape and wall zeta potential [22]. A comprehensive analysis on the up to date literature indicates that when two fluids meet at the two-liquid interface, the excess ions exist due to the ions adsorption and thus an EDL forms as a narrow region near the two-liquid interface. As a result, the corresponding electrical shear stress at liquid interface was taken into account in two-liquid model [23]-[29]. In further, the zeta potential difference at two-liquid interface caused by the difference of two fluids properties is incorporated and thus the change in electric potential at

the two-liquid interface on the velocity distribution is discussed by treating two fluids as conducting [24] [25]. In this case, the two-fluid velocity profile exhibits asymmetry around the two-liquid interface. Furthermore, the microtubes due to the relatively large pumping area are popular in practical uses [19] [20]. There is a need for manipulating working liquid with varying viscosity including biofluids and DNA solutions. The relevant studies are confined to Casson-Newtonian (inner-peripheral) model in a microtube [30], power-law-Newtonian (upper-lower) model in a microparallel [28], and viscoelastic-Newtonian (upper-lower) model in a micoparallel [31]. In [30], the inner nonconducting Casson fluid is surrounded by conducting Newtonian fluid. Compared to two-liquid flows through microparallels and rectangular microchannels, the wall effect of microtube leads to distinct transport behaviors for the inner flow and peripheral flow.

According to the knowledge of authors, the configuration manner of power-law fluid in microtubes, namely, the difference of transport features for EOF between inner power-law fluid and peripheral power-law fluid has not been carefully investigated yet. Since the microtube is frequently adopted to transport both Newtonian and non-Newtonian fluid [32] and the operation of power-law fluid in biomedical uses [33], the two-layer flow in microtubes needs to be carefully treated. The study [34] focused on the combined pressure driven and electroosmotic flow of two layer power-law fluids by evaluating velocity and flow rate at different electroosmotic characters where the coupling effect of electroosmotic characters and fluid permittivity on EOF has not been covered. In addition, according to the electrostatic theory, as two fluids interact with each other, an electric double layer and zeta potential difference occur near the two-fluid interface, which play important role on the two-fluid velocity due to the existence of both shear stress and the Maxwell stress at the two-fluid interface based on the studies [24] [35]. Therefore, in this context, the present paper aims to develop a model for two-fluid EOF of power-law fluids through a microtube in the presence of excess ions and zeta potential difference near the two-liquid interface. A fundamental understanding on the two-layer EOF under the interaction of electroosmotic characters, electric property, nonlinear constitutive relation and circular wall effect is provided by evaluating the two-fluid velocity as a function of viscosities, fluid permittivity and electroosmotic characters of two fluids. This model incorporates two-Newtonian model, Newtonian-power-law model, power-law-Newtonian model and two power-law model.

2. Mathematical Modeling

A two-layer EOF of immiscible power-law fluids in a microtube is considered. It is considered that two liquids are conducting, which are ideally symmetric electrolyte solutions with the permittivity ε_1 and ε_2, the net charge density ρ_{e1} and ρ_{e2}, the bulk ion concentration n_{01} and n_{02}, respectively. The presence of excess ions near the two-liquid interface results in the formation of EDL where the zeta potential difference is expressed by ΔZ and charge density jump is expressed by Q_s, as sketched in **Figure 1**.

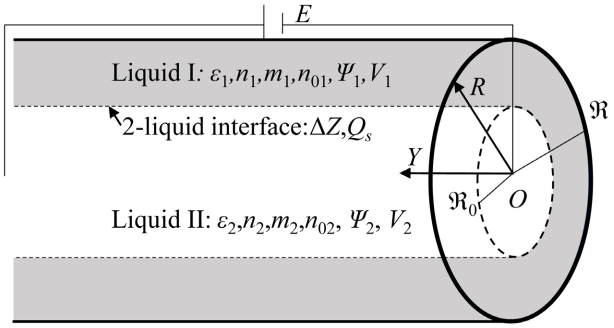

Figure 1. Schematic of two-fluid EOF of power-law fluids in a microtube with the radius of $\Re$ where the two-liquid interface is characterized by $_0$.

2.1. The Case of Two-Power-Law Fluids

An incompressible and fully developed two-layer EOF is considered. It is assumed that the length of microtube is much longer than the radius, and thus the radial velocity is ignored and the axial velocity of two-fluid can be expressed as $U_i(R)$ where $i = 1$ implies liquid I, $i = 2$ implies liquid II. In further, the two-layer flow is laminar, the gravitational force in microscales is neglected and the two-liquid interface remains stable. Considering that the EDLs near the solid surface and two-liquid interface will not overlap, and in accordance with the electrostatic theory, the net charge densities can be expressed by $\rho_{ei} = -2ezn_{0i}\sinh[ez\psi_i/(k_BT)]$ where the electric potential distribution Ψ_i inside liquid I and liquid II over the cross section of microtube can be represented by Poisson-Boltzmann (P-B) equation [3] [26]. The velocity distribution of inner power-law fluid and peripheral power-law fluid can be expressed by the modified Cauchy momentum equation as

$$(-1)^{n_i-1} m_i \frac{1}{R}\frac{\mathrm{d}}{\mathrm{d}R}\left[R\left(\frac{\mathrm{d}V_i}{\mathrm{d}R}\right)^{n_i}\right] + 2ezn_{0i}E\sinh\frac{ez\Psi_i}{k_BT} = 0 \tag{1}$$

in which e, k_B, T and z represent the elementary charge, Boltzmann number, absolute temperature and the ion valence, respectively.

The velocity distributions of two-liquid over the cross section area of microtube are subject to the axisymmetric condition around the centerline, no-slip condition at the solid interface, continuity condition at the two-liquid interface. Furthermore, the shear stress balance condition at the two-liquid interface is applied, therefore, the boundary conditions of two-layer velocity distributions are written as

$$V_1\big|_{R=\Re} = 0,\ \left.\frac{\mathrm{d}V_2}{\mathrm{d}R}\right|_{R=0} = 0,\ \left(\tau_1+\tau_{e1}\right)\big|_{R=\Re_0} = \left(\tau_2+\tau_{e2}\right)\big|_{R=\Re_0},\ \left(V_1-V_2\right)\big|_{R=\Re_0} = 0 \tag{2}$$

where the hydrodynamic shear stress τ_i and the electrical shear stress τ_{ei} of liquid i are respectively given as

$$\tau_i\big|_{R=\Re_0} = (-1)^{n-1} m_i\left(\frac{\mathrm{d}V_i}{\mathrm{d}R}\right)^{n_i}\Bigg|_{R=\Re_0},\quad \tau_{ei}\big|_{R=\Re_0} = -E\varepsilon_i\left(\frac{\mathrm{d}\Psi_i}{\mathrm{d}R}\right)\Bigg|_{R=\Re_0} \tag{3}$$

The following dimensionless parameters $\alpha = m_2\left(-U/\Re\right)^{n_2-n_1}/m_1$, $G_i = 2ezn_{0i}\Re E/\left(\rho_1 U^2\right)$, $\mu_1 = m_1\left(-U/\Re\right)^{n_1-1}$, $\mathrm{Re} = \Re\rho_1 U/\mu_1$, $U_{HS} = \varepsilon_1 k_B TE/\left(ez\mu_1\right)$, $\gamma = U_{HS}/U$, $r_0 = \Re_0/\Re$, $\zeta = ezZ/\left(k_B T\right)$, $\Delta\zeta = ez\Delta Z/\left(k_B T\right)$, $q_s = \Re ezQ_s/\left(k_B T\varepsilon_1\right)$, $\kappa = \left[e^2 z^2 n_{0i}/\left(\varepsilon_1 k_B T\right)\right]^{1/2}$, $\lambda_i = \kappa_i\Re$, $\beta = \varepsilon_2/\varepsilon_1$, $\tilde{\lambda}_2 = \lambda_2/\sqrt{\beta}$, and the following dimensionless variables $\psi_i = ez\Psi_i/\left(k_B T\right)$, $r = R/\Re$, $v_i = V_i/U$ have been introduced. Consequently, under the framework of Debye-Hückel approximation, namely $\sinh\psi \approx \psi$ for $|\psi| \le 1$, the dimensionless modified Cauchy momentum equation and the boundary conditions are derived as

$$\frac{1}{r}\frac{\mathrm{d}}{\mathrm{d}r}\left[r\left(\frac{\mathrm{d}v_1}{\mathrm{d}r}\right)^{n_1}\right] - G_1\,\mathrm{Re}\,\psi_1\left(r\right) = 0 \quad \text{for} \quad r_0 \le r \le 1 \tag{4}$$

$$\alpha\frac{1}{r}\frac{\mathrm{d}}{\mathrm{d}r}\left[r\left(\frac{\mathrm{d}v_2}{\mathrm{d}r}\right)^{n_2}\right] - G_2\,\mathrm{Re}\,\psi_2\left(r\right) = 0 \quad \text{for} \quad 0 \le r \le r_0 \tag{5}$$

$$v_1\big|_{r=1} = 0,\ \left.\frac{\mathrm{d}v_2}{\mathrm{d}r}\right|_{r=0} = 0,\ \left(v_1 - v_2\right)\big|_{r=r_0} = 0,$$

$$\left[\left(\frac{\mathrm{d}v_1}{\mathrm{d}r}\right)^{n_1} - \gamma\frac{\mathrm{d}\psi_1}{\mathrm{d}r}\right]\Bigg|_{r=r_0} = \left[\alpha\left(\frac{\mathrm{d}v_2}{\mathrm{d}r}\right)^{n_2} - \beta\gamma\frac{\mathrm{d}\psi_2}{\mathrm{d}r}\right]\Bigg|_{r=r_0} \tag{6}$$

where U, U_{HS}, ρ_1, G_i and Re represent the reference velocity, Helmholtz-Smoluchowski electroosmotic velocity, density of peripheral power-law fluid I, conversion of electrical energy to fluid kinetic energy of liquid i (i = 1, 2) and Reynolds number, respectively. The dimensionless two-fluid electric potential distribution is given as [34]

$$\psi_1\left(r\right) = AI_0\left(\lambda_1 r\right) + BK_0\left(\lambda_1 r\right) \tag{7}$$

$$\psi_2\left(r\right) = CI_0\left(\tilde{\lambda}_2 r\right) \tag{8}$$

where the coefficients are presented in Appendix for conciseness and readability. I_ν and K_ν imply ν-th order modified Bessel function of first kind and second kind (ν = 0, 1), respectively. $1/\kappa_i$ implies the Debye length of EDL inside liquid i (i = 1, 2), and β indicates fluid permittivity ratio. Specifically, λ_1 denotes the electrokinetic width of EDL near the solid interface, and λ_2 denotes the electrokinetic width of EDL near the two-liquid interface.

Solving Equations (4)-(8) yields the semi-analytical solutions for the two fluid velocities as below

$$v_1\left(r\right) = \int_1^r \left\{\frac{G_1\,\mathrm{Re}}{\lambda_1}\left[AI_1\left(\lambda_1\tilde{r}\right) - BK_1\left(\lambda_1\tilde{r}\right)\right]\right\}^{1/n_1}\mathrm{d}\tilde{r} \quad \text{for} \quad r_0 \le r \le 1 \tag{9}$$

$$v_2\left(r\right) = \int_{r_0}^r \left\{\frac{G_2\,\mathrm{Re}}{\alpha\tilde{\lambda}_2}CI_1\left(\tilde{\lambda}_2\tilde{r}\right)\right\}^{1/n_2}\mathrm{d}\tilde{r} + v_1\left(r_0\right) \quad \text{for} \quad 0 \le r \le r_0 \tag{10}$$

Eventually one obtains the two-fluid velocity which is expressed as v for $0 \le r \le 1$ by incorporating v_1 and v_2. It can be seen from the expressions of electric

potential distribution given by Equation (7) and Equation (8) that electric potential distribution and thus the velocity distribution experience rapid change near the interfaces, therefore, when numerically solving Equation (9) and Equation (10), the technique of variation substitution $t = a + b\exp(kr)$ is adopted to obtain denser points near the interfaces. The specific procedure of substitution is neglected for conciseness. Subsequently, the composite trapezoidal method and Matlab software have been used to obtain the numerical two-layer velocity distributions.

2.2. The Case of Two-Newtonian Fluids

To validate the numerical methods mentioned above, the analytical velocities of two-layer flow of Newtonian fluids need to be solved. Setting $n_1 = n_2 = 1$, one obtains the momentum equations for two-layer flow as below

$$\frac{1}{r}\frac{\mathrm{d}}{\mathrm{d}r}\left[r\left(\frac{\mathrm{d}v_1}{\mathrm{d}r}\right)\right] - G_1 \,\mathrm{Re}\,\psi_1(r) = 0 \quad \text{for} \quad r_0 \le r \le 1 \tag{11}$$

$$\frac{1}{r}\frac{\mathrm{d}}{\mathrm{d}r}\left[r\left(\frac{\mathrm{d}v_2}{\mathrm{d}r}\right)\right] - G_2 \,\mathrm{Re}\,\psi_2(r) = 0 \quad \text{for} \quad 0 \le r \le r_0 \tag{12}$$

$$v_1\big|_{r=1} = 0, \quad \left.\frac{\mathrm{d}v_2}{\mathrm{d}r}\right|_{r=0} = 0, \quad \left(v_1 - v_2\right)\big|_{r=r_0} = 0,$$

$$\left[\frac{\mathrm{d}v_1}{\mathrm{d}r} - \gamma\frac{\mathrm{d}\psi_1}{\mathrm{d}r}\right]\Bigg|_{r=r_0} = \left[\frac{\mathrm{d}v_2}{\mathrm{d}r} - \beta\gamma\frac{\mathrm{d}\psi_2}{\mathrm{d}r}\right]\Bigg|_{r=r_0} \tag{13}$$

Solving Equations (11)-(13) yields the following analytical solutions for velocities

$$v_1^N(r) = \frac{G_1 \,\mathrm{Re}}{\lambda_1^2}\psi_1(r) + D_1 \quad \text{for} \quad r_0 \le r \le 1 \tag{14}$$

$$v_2^N(r) = \frac{G_2 \,\mathrm{Re}}{\lambda_2^2}\psi_2(r) + D_2 \quad \text{for} \quad 0 \le r \le r_0 \tag{15}$$

where $D_1 = -\dfrac{G_1 \,\mathrm{Re}\,\zeta}{\lambda_1^2}$ and $D_2 = v_1(r_0) - \dfrac{G_2 \,\mathrm{Re}}{\lambda_2^2}\psi_2(r_0)$.

3. Results and Discussions

Two-layer EOF of power-law fluids is parametrically studied by evaluating the two-liquid velocities at different flow behavior index of peripheral fluid I n_1, flow behavior index of inner fluid II n_2, electrokinetic width of EDL near the solid interface λ_1, electrokinetic width of EDL near the two-liquid interface λ_2, zeta potential near the solid interface ζ, zeta potential difference near the two-liquid interface $\Delta\zeta$, the fluid permittivity ratio β. The physical parameters take the following values $E = 1 \times 10^4$ V/m, $N_A = 6.02 \times 10^{23}$/mol, $e = 1.6 \times 10^{-19}$ C, $k_B = 1.38 \times 10^{-23}$ J/K, $\rho = 1 \times 10^3$ kg/m^3, $m_1 = m_2 = 9 \times 10^{-4}$ N·m^{-2}·s^n, $\varepsilon_1 = 7.08 \times 10^{-10}$ C^2/Jm, $T = 293$ K, $\Re = 100$ μm, $r_0 = 0.5$, $U = 1 \times 10^{-4}$ m/s, respectively [23] [24] [36].

For two-layer Newtonian fluid flow, the numerical solutions of two-layer velocity obtained from Equations (9) and (10) are compared with the corresponding analytical solutions of velocity presented by Equations (11) and (12) in **Figure 2(a)**. When n_0 approaches to 1, the numerical solutions for single-layer velocity are obtained from Equation (10) by using the same numerical integration method and they are compared with the existing data from [32] in **Figure 2(b)**. The numerical velocities at different parameters show good agreement with the analytical velocities and thus it proves that the numerical methods applied are valid which can be used to solve velocity of two-layer flows of power-law fluids.

The two-layer velocity distributions over the cross section area of microtube at different flow behavior index of peripheral fluid n_1 and zeta potential difference $\Delta\zeta$ are presented in **Figure 3** where the inner fluid is shear thickening fluid. For a prescribed $\Delta\zeta$, the increase in n_1 enhances the viscosity of peripheral fluid, leading to the reduction of two-liquid velocity in a whole. For a given peripheral fluid, namely when n_1 is fixed, the zeta potential difference $|\Delta\zeta|$ augments the inner fluid flow and affects the peripheral flow near the liquid interface, meaning that the EDL effect at liquid interface serves as a driving force for the inner fluid.

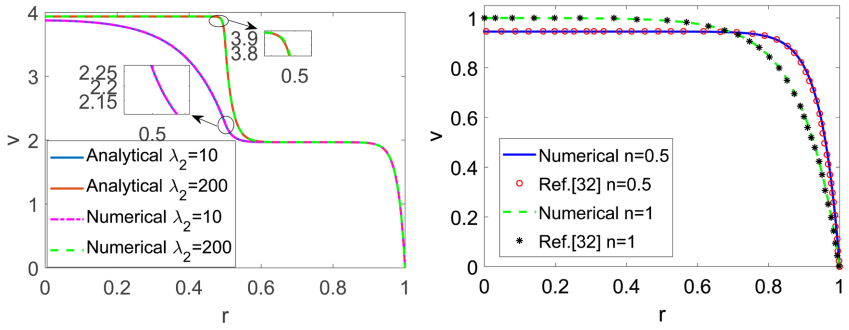

Figure 2. (a) The comparison between the numerical velocity and analytical velocity for two-layer EOF of Newtonian fluids and (b) the comparison between the numerical velocity when ($n_0 \to 1$), and the existing date in [32] for single-layer EOF of power-law fluid.

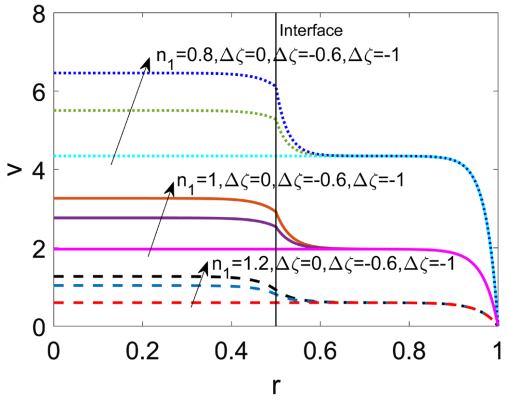

Figure 3. The comparison of two-liquid velocity profiles v at different flow behavior index of peripheral fluid I n_1 and at different zeta potential difference $\Delta\zeta$ when $\lambda_1 = \lambda_2 = 50$, $q_s = 0$, $\beta = 1$, $\zeta = -1$.

As the flow behavior index of peripheral fluid n_1 decreases, the effect of $\Delta\zeta$ on inner fluid flow gets more and more noticeable. To note, when $q_s = 0$ and $\Delta\zeta$ becomes zero, namely the EDL effect near the two-liquid interface vanishes, accordingly, the inner velocity obtained from the EDL effect near the two-liquid interface vanishes, and the inner velocity becomes entirely dependent on the peripheral fluid flow. It can be explained by the fact that the circular effect, resulting from the axisymmetric condition of velocity around centerline and velocity continuity at the liquid interface in a microtube quantified as the constant term in Equation (10), drives the inner fluid with the same velocity as the peripheral velocity at the liquid interface.

As shown in Figure 4, the variations of two-fluid velocity with flow behavior index of inner fluid n_2 are presented for different zeta potential difference at the liquid interface $\Delta\zeta$. When $q_s = 0$ and $\Delta\zeta = 0$, regardless of the inner fluid type, the inner fluid will achieve the identical velocity to the peripheral fluid near the liquid interface due to the circular effect. For a nonzero and prescribed $\Delta\zeta$, the increase in n_2 clogs the inner flow and has no influence on the peripheral fluid flow. The increase in $|\Delta\zeta|$ intensifies the EDL effect near the two-liquid interface and thus enhances the inner fluid velocity. Therefore, the electric property of two-liquid interface quantified by $\Delta\zeta$, exerts influence on the inner fluid as a whole and the peripheral fluid near the two-liquid interface. The effect of $\Delta\zeta$ becomes more remarkable when inner fluid changes from shear thickening to shear thinning.

The two-liquid velocity profiles for different zeta potential near the solid interface ζ are plotted in Figure 5. It shows that with the increase of $|\zeta|$, the electroosmotic force near the solid interface of channel wall gets intensified, as a result the peripheral velocity and the inner velocity increases. Moreover, $\zeta = 0$ corresponds to the vanishment of driving force of peripheral fluid, therefore, the peripheral bulk fluid is static and the fluid near liquid interface is dragged by the electrical shear stress since the continuity condition of shear stress is applied at two-liquid interface.

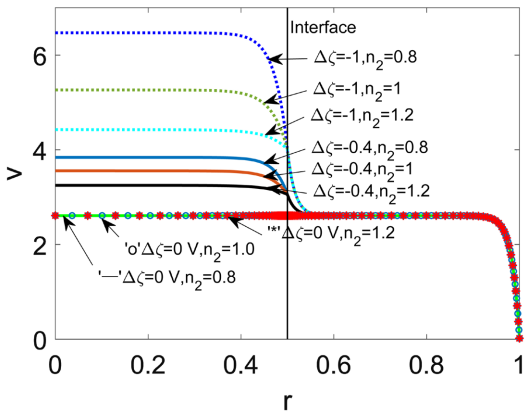

Figure 4. The comparison of two-liquid velocity profiles v at different flow behavior index n_2 of fluid II and at different zeta potential difference $\Delta\zeta$ when $\lambda_1 = 50$, $\lambda_2 = 30$, $q_s = 0$, $\beta = 1$, $\zeta = -0.6$.

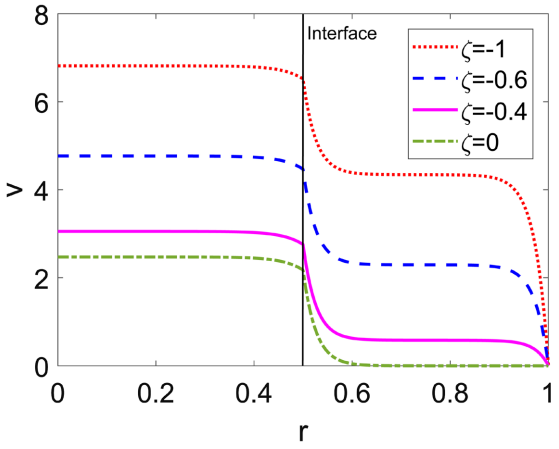

Figure 5. The comparison of velocity profiles v at different zeta potential at the solid interface ζ when $\Delta\zeta = 1$, $\lambda_2 = 30$, $q_s = 5$, $\beta = 1$, $n_1 = 0.8$, $n_2 = 1.2$.

The two-liquid velocity profiles for different electrokinetic width of EDL near the solid interface λ_1 are presented in Figure 6. The increase in λ_1 augments the flow of peripheral shear thinning fluid and thus the constant term in Equation (10) is increased, thereby the inner shear thickening fluid acquires a higher velocity. Consistent to single-fluid EOF, a larger λ_1 will alters the peripheral velocity profile from parabolic to plug-like. A smaller λ_1 means wider distribution of electroosmotic force inside peripheral fluid, leading to relatively gradual change of velocity profile in peripheral flow.

The two-liquid velocity profiles for different electrokinetic width of EDL near the liquid interface λ_2 are plotted in Figure 7. The EOF flow of inner shear thickening fluid is augmented in a whole and exhibits plug-like profile as λ_2 increases. Meanwhile, the peripheral shear thinning fluid is weakly influenced in the vicinity of liquid interface by the change in λ_2.

The two-liquid velocity profiles for different fluid II permittivity ratio ε_2 are compared in Figure 8. Specifically, the value of ε_2 is improved by enhancing β and keeping the fluid I permittivity ε_1 unchanged. The increase of inner fluid II permittivity leads to the enhancement of the inner fluid II velocity, which shows little influence on the peripheral fluid I velocity. The variation of two-liquid velocity with λ_2 and ε_2 as shown in Figure 7 and Figure 8 can be explained by the fact that the change in λ_2 and ε_2 intensifies the electric potential in the vicinity of liquid interface, which enhances the electroosmotic force near the two-liquid interface, in further, the inner bulk fluid flow.

In Figure 9, the two-liquid velocity profiles for different fluid I permittivity ε_1 are presented. Specifically, the value of ε_1 is improved by reducing β and simultaneously keeping the fluid II permittivity unchanged. As compared to Figure 8, the change in fluid I permittivity ε_1 accounts for the uniform change of two-liquid velocity due to the circular effect of microtube, therefore, the change in electric property of peripheral fluid I dominates on the two-liquid velocity by affecting the driving force of two-fluid system.

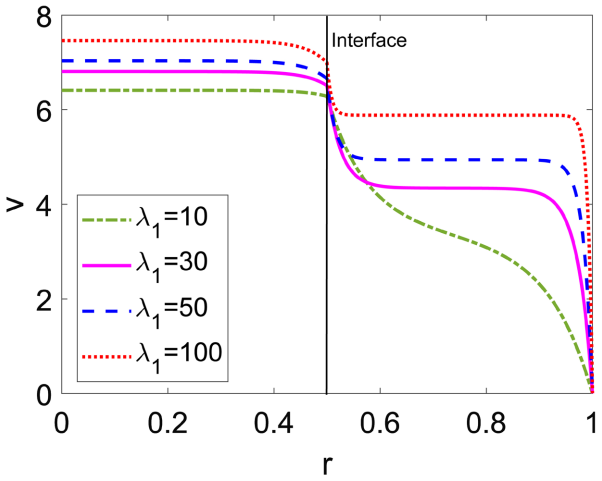

Figure 6. The comparison of velocity profiles v at different electrokinetic width of EDL near the solid interface λ_1 when $\lambda_2 = 30$, $q_s = 5$, $\beta = 1$, $\Gamma = 0$, $n_1 = 0.8$, $n_2 = 1.2$, $\zeta = \Delta\zeta = 1$.

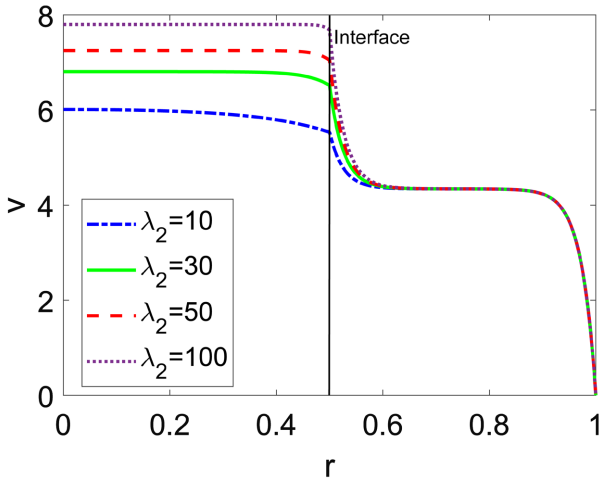

Figure 7. The comparison of velocity profiles v at different electrokinetic width of EDL near the liquid interface λ_2 when $\lambda_1 = 30$, $q_s = 5$, $n_1 = 0.8$, $n_2 = 1.2$, $\Delta\zeta = \zeta = -1$.

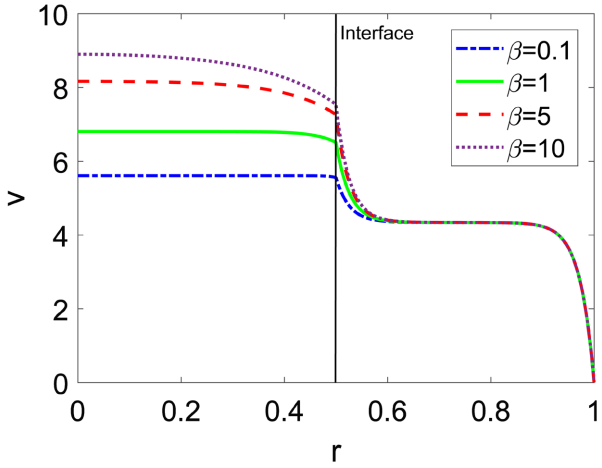

Figure 8. The comparison of velocity profiles v at different fluid permitivity ε_2 when $\varepsilon_1 = 7.08 \times 10^{-10}$, $\lambda_1 = \lambda_2 = 30$, $q_s = 5$, $n_1 = 0.8$, $n_2 = 1.2$, $\Delta\zeta = \zeta = -1$.

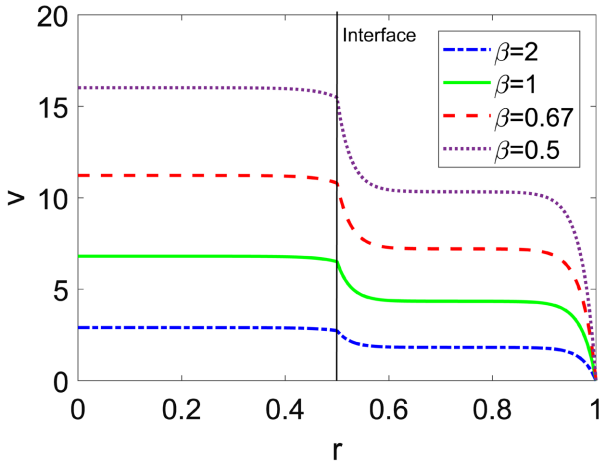

Figure 9. The comparison of velocity profiles v at differnent ε_1 when $\varepsilon_2 = 7.08 \times 10^{-10}$, $\lambda_1 = \lambda_2 = 30$, $q_s = 5$, $n_1 = 0.8$, $n_2 = 1.2$, $\Delta\zeta = \zeta = -1$.

4. Conclusions

The two-layer EOF of immiscible power-law fluids in the presence of the zeta potential difference near the two-liquid interface has been studied. The inner fluid and the peripheral fluid are represented by power-law model; thereby the effect of power-law rheology on the two-layer flow in a microtube has been investigated. Specifically, the two-liquid velocity profile is evaluated as a function of viscosity, electric property of both inner and peripheral fluid, as well as the electric property of two-liquid interface.

The inner flow is not only dependent on the viscosity and electric property of fluid II represented by n_2, λ_2, ε_2 and the electric property of liquid interface $\Delta\zeta$, but also the viscosity and electric property of fluid I quantified by n_1, λ_1, ζ, ε_2. In contrast, the viscosity of fluid II shows no influence on peripheral fluid. The electric properties of fluid II and that of two-liquid interface only affect the velocity of peripheral fluid near the liquid interface. It is noteworthy that the influence of fluid permitivity on velocity profile outweighs the influence of electrokinetic width. Particularly, the increase in permitivity of peripheral fluid not only alters the peripheral flow but also significantly accelerates the inner flow. Therefore, in engineering, the fluid with high permitivity can be used as peripheral driving liquid. In the meantime, the two-layer flow can be effectively manipulated by adjusting permitivities of two fluids. Moreover, due to the existence of circular effect, the peripheral flow assists in the inner flow. Irrespective of the configuration manner of power-law fluid in a microtube, the shear thinning fluid is more sensitive to the change in $\Delta\zeta$. When $q_s > 0$ and $\Delta\zeta < 0$, the inner fluid II will achieve higher velocity than that of peripheral fluid I under the coupling effect of the external electric field and EDL effect. The peripheral fluid is driven by the electroosmotic force resulting from EDL effect near the channel wall, and the inner fluid is driven by the combined effect of electroosmtotic force owing to the EDL effect near the two-liquid interface and the peripheral flow. Therefore, in practical uses, irrespective of fluid type, the low EO mobility fluids can be

placed as in inner layer and assisted by the peripheral shear thinning fluid flow.

Acknowledgements

This work was supported by the Guangdong Basic and Applied Basic Research Foundation 2021A1515012371, the National Natural Science Foundation of China, grant number 11902082, the Talent Introduction Foundation of Guangdong University of Petrochemical Technology, grant number 2018rc16, the Scientific Research Foundation of Universities in Guangdong Province for Young Talents, grant number 2018KQNCX165, the Scientific Research Foundation of Guangdong University of Petrochemical Technology, grant number 513040, and the Municipal Science and Technology Program of Maoming, grant number 2019408.

Conflicts of Interest

The author declares no conflicts of interest regarding the publication of this paper.

References

[1] Figeys, D. and Pinto, D. (2000) Lab-on-a-Chip: A Revolution in Biological and Medical Sciences. *Analytical Chemistry*, **72**, 330A-335A. https://doi.org/10.1021/ac002800y

[2] Laser, D.J. and Santiago, J.G. (2004) A Review of Micropumps. *Journal of Micromechanics and Microengineering*, **14**, R35-R64. https://doi.org/10.1088/0960-1317/14/6/R01

[3] Bruus, H. (2008) Theoretical Microfluidics. Oxford University Press, Oxford.

[4] Kang, Y.J., Yang, C. and Huang, X.Y. (2002) Dynamic Aspects of Electroosmotic Flow in a Cylindrical Microcapillary. *International Journal of Engineering Science*, **40**, 2203-2221. https://doi.org/10.1016/S0020-7225(02)00143-X

[5] Kang, Y.J., Yang, C. and Huang, X.Y. (2002) Electroosmotic Flow in a Capillary Annulus with High Zeta Potentials. *Journal of Colloid and Interface Science*, **253**, 285-294. https://doi.org/10.1006/jcis.2002.8453

[6] Bianchi, F., Ferrigno, R. and Girault, H.H. (2000) Finite Element Simulation of an Electroosmotic-Driven Flow Division at a t-Junction of Microscale Dimensions. *Analytical Chemistry*, **72**, 1987-1993. https://doi.org/10.1021/ac991225z

[7] Marcos; Yang, C., Wong, T.N. and Ooi, K.T. (2004) Dynamic Aspects of Electroosmotic Flow in Rectangular Microchannels. *International Journal of Engineering Science*, **42**, 1459-1481. https://doi.org/10.1016/j.ijengsci.2003.07.012

[8] Moghadam, A.J. (2012) An Exact Solution of ac Electro-Kinetic-Driven Flow in a Circular Micro-Channel. *European Journal of Mechanics—B/Fluids*, **34**, 91-96. https://doi.org/10.1016/j.euromechflu.2012.03.006

[9] Moghadam, A.J. (2015) Thermal Characteristics of Time-Periodic Electroosmotic Flow in a Circular Microchannel. *Heat and Mass Transfer*, **51**, 1461-1473. https://doi.org/10.1007/s00231-015-1513-7

[10] Das, S. and Chakraborty, S. (2006) Analytical Solutions for Velocity, Temperature and Concentration Distribution in Electroosmotic Microchannel Flows of a Non-Newtonian Bio-Fluid. *Analytica Chimica Acta*, **559**, 15-24.

https://doi.org/10.1016/j.aca.2005.11.046

[11] Deng, S.Y., Jian, Y.J., Bi, Y.H., Chang, L., Wang, H.J. and Liu, Q.S. (2012) Unsteady Electroosmotic Flow of Power-Law Fluid in a Rectangular Microchannel. *Mechanics Research Communications*, **39**, 9-14. https://doi.org/10.1016/j.mechrescom.2011.09.003

[12] Zhu, Q.Y., Deng, S.Y. and Chen, Y.Q. (2014) Periodical Pressure-Driven Electrokinetic Flow of Power-Law Fluids through a Rectangular Microchannel. *Journal of Non-Newtonian Fluid Mechanics*, **203**, 38-50. https://doi.org/10.1016/j.jnnfm.2013.10.003

[13] Misra, J.C., Shit, G.C., Chandra, S. and Kundu, P.K. (2011) Electro-Osmotic Flow of a Viscoelastic Fluid in a Channel: Applications to Physiological Fluid Mechanics. *Applied Mathematics & Computation*, **217**, 7932-7939. https://doi.org/10.1016/j.amc.2011.02.075

[14] Jiménez, E., Escandón, J., Bautista, O. and Méndez, F. (2016) Start-Up Electroosmotic Flow of Maxwell Fluids in a Rectangular Microchannel with High Zeta Potentials. *Journal of Non-Newtonian Fluid Mechanics*, **227**, 17-29. https://doi.org/10.1016/j.jnnfm.2015.11.003

[15] Ng, C.O. (2013) Combined Pressure-Driven and Electroosmotic Flow of Casson Fluid through a Slit Microchannel. *Journal of Non-Newtonian Fluid Mechanics*, **198**, 1-9. https://doi.org/10.1016/j.jnnfm.2013.03.003

[16] Mondal, A. and Shit, G.C. (2017) Transport of Magneto-Nanoparticles during Electro-Osmotic Flow in a Micro-Tube in the Presence of Magnetic Field for Drug Delivery Application. *Journal of Magnetism and Magnetic Materials*, **442**, 319-328. https://doi.org/10.1016/j.jmmm.2017.06.131

[17] Si, D.Q., Jian, Y.J., Chang, L. and Liu, Q.S. (2016) Unsteady Rotating Electroosmotic Flow through a Slit Microchannel. *Journal of Mechanics*, **32**, 603-611. https://doi.org/10.1017/jmech.2016.9

[18] Datta, S., Ghosal, S. and Patankar, N.A. (2006) Electroosmotic Flow in a Rectangular Channel with Variable Wall Zeta-Potential: Comparison of Numerical Simulation with Asymptotic Theory. *Electrophoresis*, **27**, 611-619. https://doi.org/10.1002/elps.200500618

[19] Kwon, K., Park, C.-W. and Kim, D. (2012) High-Flowrate, Compact Electroosmotic Pumps with Porous Polymer Track-Etch Membranes. *Sensors and Actuators A: Physical*, **175**, 108-115. https://doi.org/10.1016/j.sna.2011.12.050

[20] Yao, S. and Santiago, J.G. (2003) Porous Glass Electroosmotic Pumps: Theory. *Journal of Colloid and Interface Science*, **268**, 133-142. https://doi.org/10.1016/S0021-9797(03)00731-8

[21] Brask, A., Goranovic, G. and Bruus, H. (2003) Electroosmotic Pumping of Nonconducting Liquids by Viscous Drag from a Secondary Conducting Liquid. *Proceedings NANOTECH*, Vol. 1, 190-193.

[22] Qi, C. and Ng, C.-O. (2018) Electroosmotic Flow of a Two-Layer Fluid in a Slit Channel with Gradually Varying Wall Shape and Zeta Potential. *International Journal of Heat and Mass Transfer*, **119**, 52-64. https://doi.org/10.1016/j.ijheatmasstransfer.2017.11.114

[23] Gao, Y.D., Wong, T.N., Yang, C. and Ooi, K.T. (2005) Transient Two-Liquid Electroosmotic Flow with Electric Charges at the Interface. *Colloids and Surfaces A*, **266**, 117-128. https://doi.org/10.1016/j.colsurfa.2005.05.068

[24] Su, J., Jian, Y.J., Chang, L. and Liu, Q.S. (2013) Transient Electro-Osmotic and Pressure Driven Flows of Two-Layer Fluids through a Slit Microchannel. *Acta Me-*

chanica Sinica, **29**, 534-542. https://doi.org/10.1007/s10409-013-0051-0

[25] Choi, W., Sharma, A., Qian, S., Lim, G. and Joo, S.W. (2011) On Steady Two-Fluid Electroosmotic Flow with Full Interfacial Electrostatics. *Journal of Colloid and Interface Science*, **357**, 521-526. https://doi.org/10.1016/j.jcis.2011.01.107

[26] Moghadam, A.J. (2016) Two-Fluid Electrokinetic Flow in a Circular Microchannel. *International Journal of Engineering*, *Transactions A*, **29**, 1469-1477. https://doi.org/10.5829/idosi.ije.2016.29.10a.18

[27] Afonso, A.M., Alves, M.A. and Pinho, F.T. (2013) Analytical Solution of Two-Fluid Electro-Osmotic Flows of Viscoelastic Fluids. *Journal of Colloid and Interface Science*, **395**, 277-286. https://doi.org/10.1016/j.jcis.2012.12.013

[28] Huang, Y., Li, H.W. and Wong, T.N. (2014) Two Immiscible Layers of Electro-Osmotic Driven Flow with a Layer of Conducting Non-Newtonian Fluid. *International Journal of Heat and Mass Transfer*, **74**, 368-375. https://doi.org/10.1016/j.ijheatmasstransfer.2014.02.068

[29] Moghadam, A.J. and Akbarzadeh, P. (2019) AC Two-Immiscible-Fluid EOF in a Microcapillary. *Journal of the Brazilian Society of Mechanical Sciences and Engineering*, **41**, 194-194. https://doi.org/10.1007/s40430-019-1702-2

[30] Liu, M., Liu, Y., Guo, Q. and Yang, J. (2009) Modeling of Electroosmotic Pumping of Nonconducting Liquids and Biofluids by a Two-Phase Flow Method. *Journal of ElectroAnalytical Chemistry*, **636**, 86-92. https://doi.org/10.1016/j.jelechem.2009.09.015

[31] Xie, Z. and Jian, Y. (2018) Entropy Generation of Magnetohydrodynamic Electroosmotic Flow in Two-Layer Systems with a Layer of Non-Conducting Viscoelastic Fluid. *International Journal of Heat and Mass Transfer*, **127**, 600-615. https://doi.org/10.1016/j.ijheatmasstransfer.2018.07.065

[32] Moghadam, A.J. (2013) Electrokinetic-Driven Flow and Heat Transfer of a Non-Newtonian Fluid in a Circular Microchannel. *Journal of Heat Transfer*, **135**, Article ID: 021705. https://doi.org/10.1115/1.4007542

[33] Patel, M., Harish Kruthiventi, S.S. and Kaushik, P. (2020) Rotating Electroosmotic Flow of Power-Law Fluid through Polyelectrolyte Grafted Microchannel. *Colloids and Surfaces B*: *Biointerfaces*, **193**, Article ID: 111058. https://doi.org/10.1016/j.colsurfb.2020.111058

[34] Deng, S.Y., Xiao, T. and Wu, S.M. (2021) Two-Layer Combined Electroosmotic and Pressure-Driven Flow of Power-Law Fluids in a Circular Microcapillary. *Colloids and Surfaces A*, **610**, Article ID: 125727. https://doi.org/10.1016/j.colsurfa.2020.125727

[35] Zheng, J.X. and Jian, Y.J. (2018) Rotating Electroosmotic Flow of Two-Layer Fluids through a Microparallel Channel. *International Journal of Mechanical Sciences*, **136**, 293-302. https://doi.org/10.1016/j.ijmecsci.2017.12.039

[36] Deng, S.Y. (2017) The Parametric Study of Electroosmotically Driven Flow of Power-Law Fluid in a Cylindrical Microcapillary at High Zeta Potential. *Micromachines*, **8**, 344-357. https://doi.org/10.3390/mi8120344